THE JOURNAL OF PHYSICAL CHEMISTRY A

Article

pubs.acs.org/JPCA

Photodissociation Studies of the Electronic and Vibrational Spectroscopy of $Ni^+(H_2O)$

Jennifer S. Daluz,† Abdulkadir Kocak, and Ricardo B. Metz*

Department of Chemistry, University of Massachusetts Amherst, Amherst, Massachusetts 01003, United States

ABSTRACT: The electronic spectrum of $Ni^+(H_2O)$ has been measured from 16200 to 18000 cm^{-1} using photofragment spectroscopy. Transitions to two excited electronic states are observed; they are sufficiently long-lived that the spectrum is vibrationally and partially rotationally resolved. An extended progression in the metal−ligand stretch is observed, and the absolute vibrational quantum numbering is assigned by comparing isotopic shifts between $^{58}Ni^+(H_2O)$ and $^{60}Ni^+(H_2O)$. Time-dependent density functional calculations aid in assigning the spectrum. Two electronic transitions are observed, from the $^2A_1$ ground state (which correlates to the ^2D, $3d^9$ ground state of Ni^+) to the 3^2A_1 and 2^2A_2 excited states. These states are nearly degenerate and correlate to the ^2F, $3d^84s$ excited state of Ni^+. Both transitions are quite weak, but surprisingly, the transition to the $^2A_2$ state is stronger, although it is symmetry-forbidden. The $3d^84s$ states of Ni^+ interact less strongly with water than does the ground state; therefore, the excited states observed are less tightly bound and have a longer metal−ligand bond than the ground state. Calculations at the CCSD(T)/aug-cc-pVTZ level predict that binding to Ni^+ increases the H−O−H angle in water from 104.2 to 107.5° as the metal removes electron density from the oxygen lone pairs. The photodissociation spectrum shows well-resolved rotational structure due to rotation about the Ni−O axis. This permits determination of the spin rotation constants $\varepsilon_{\alpha\alpha}'' = -12$ cm^{-1} and $\varepsilon_{\alpha\alpha}' = -3$ cm^{-1} and the excited state rotational constant $A' = 14.5$ cm^{-1}. This implies a H−O−H angle of 104 ± 1° in the 2^2A_2 excited state. The O−H stretching frequencies of the ground state of $Ni^+(H_2O)$ were measured by combining IR excitation with visible photodissociation in a double resonance experiment. The O−H symmetric stretch is $\nu_1'' = 3616.5$ cm^{-1}; the antisymmetric stretch is $\nu_5'' = 3688$ cm^{-1}. These values are 40 and 68 cm^{-1} lower, respectively, than those in bare H_2O.

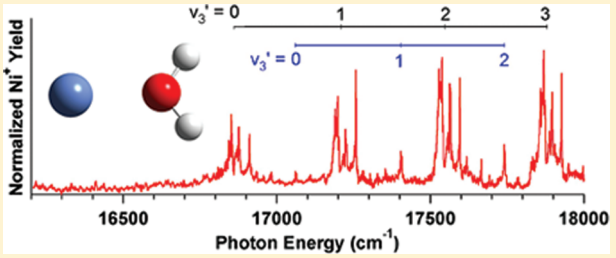

1. INTRODUCTION

Metal ion−water complexes have been the subject of numerous experimental and theoretical studies due to the importance of metal−water interactions in solvation, homogeneous catalysis, and biological processes. In some cases, a H_2O ligand is key to the enzyme mechanism. For example, urease catalyzes the reaction of urea with water to form carbon dioxide and ammonia. The active site contains two nickel atoms, one of which is coordinated to H_2O.[1] In the proposed mechanism, this water is deprotonated and subsequently reacts with the urea.[2] Gas-phase studies of metal ion−water complexes permit the detailed investigation of this fundamental noncovalent interaction and its dependence on the charge and electron configuration of the metal, as well as how interaction with the metal affects the structure and bonding in the water ligand.[3]

There have been a few previous studies investigating noncovalent Ni^+ complexes in the gas phase. Dalleska et al. used guided ion beam methods to measure binding energies of the first four H_2O molecules to the first row transition-metal ions M^+. They found binding energies to be 15100, 14060, 5650, and 4300 cm^{-1} for $Ni^+(H_2O)_n$, n = 1−4, respectively.[4] Brucat and co-workers have measured electronic spectra of complexes of Ni^+ with Ar, N_2O, and CO_2 using photofragment spectroscopy.[5] They determined binding energies and, in some cases, vibrational frequencies in the excited electronic state. As part of a series of studies of $M^+(H_2O)_n$ complexes by Duncan and co-workers,[6] Walters et al. measured vibrational spectra of $Ni^+(H_2O)_n$ clusters, n = 1−25, in the O−H stretching region via IR photofragment spectroscopy.[6c] Because the energy required to break the $Ni^+(H_2O)_{n-1}$−H_2O bond is greater than that available with one IR photon for n = 1−4, they studied $Ni^+(H_2O)_n(Ar)_m$ instead, monitoring absorption via argon loss. It is possible that the argon tag may perturb the O−H stretches. In addition, the rotational structure of $Ni^+(H_2O)(Ar)_2$, the smallest cluster studied, is very different from that of $Ni^+(H_2O)$. Electronic spectra of $M^+(H_2O)$ complexes have been reported for the alkaline earth metals M = Mg,[7,8] Ca,[9,10] and Sr[11] and for the transition metals V,[12] Co,[13] and Zn,[14] all measured by photofragment spectroscopy.

For $Ni^+(H_2O)$, which has a Ni^+−H_2O bond strength[4] of 1.87 ± 0.03 eV (15100 ± 200 cm^{-1}), one photon with wavelength λ < 662 nm has sufficient energy to dissociate the molecule. Therefore, we are able to measure the electronic spectrum of gas-phase $Ni^+(H_2O)$ using photofragment spectroscopy. The vibrational spectrum of $Ni^+(H_2O)$ is measured by combining IR excitation with visible photodissociation in a double

Received: November 21, 2011
Revised: January 3, 2012

dx.doi.org/10.1021/jp211220v | J. Phys. Chem. A XXXX, XXX, XXX−XXX

resonance experiment. From the electronic and vibrational spectra, we determine how the electronic configuration of the Ni^+ affects the Ni^+-H_2O interaction and how binding to the Ni^+ perturbs the O−H bonds and the H−O−H angle in the complex.

2. EXPERIMENTAL SETUP

The experiments take place in a dual time-of-flight mass spectrometer, which has been described in detail.[15] Nickel ions are formed via laser ablation of a rotating, translating nickel rod. They then react with a gas mixture of 0.14% H_2O seeded in helium to produce $Ni^+(H_2O)$ complexes. The molecules expand into vacuum, cooling to rotational temperatures of 5−20 K. The ion beam is then skimmed, accelerated, and later rereferenced to ground potential. The ions of interest are mass-selected using a pulsed mass gate and are dissociated at the turning point of the reflectron by a visible dye laser. In the double resonance experiments, an IR laser is also used. Unless otherwise noted, experiments are carried out on the most abundant isotope, $^{58}Ni^+(H_2O)$. The masses of the fragment ions are determined by their flight times. The dissociation efficiency is improved by a multipass system,[16] which enables the laser beams to pass through the ion beam 21 times. The dye laser is a Continuum ND60, pumped by a Continuum Surelite I-20 Nd:YAG laser. It produces >10 mJ/pulse and is tunable from 545 to ∼800 nm with a line width of 0.1 cm^{-1}. The IR laser system is a LaserVision OPO/OPA pumped by a Continuum Powerlite 8020. It is tunable from 2200 to >4000 cm^{-1}, produces ∼12 mJ/pulse near 3700 cm^{-1}, and has a line width of 1.8 cm^{-1}. In the double resonance experiments, the IR laser fires 40 ns before the visible laser. The resulting signal is collected using a gated integrator and a LabView based program.

3. RESULTS AND ANALYSIS

A. Electronic Spectroscopy: Vibrational Structure. The electronic and vibrational spectra of $Ni^+(H_2O)$ were measured using photofragment spectroscopy. Figure 1 shows a survey photodissociation spectrum of $Ni^+(H_2O)$. The onset occurs at ∼16840 cm^{-1}, and the spectrum consists of an extended progression of vibrational bands spaced by ∼340 cm^{-1}. In addition, each vibrational band consists of at least three peaks separated by ∼30 cm^{-1}, characteristic[9] of rotational structure in a perpendicular transition of a prolate top with a large A rotational constant of ∼15 cm^{-1}. The rotational structure will be discussed in detail later. The only fragment observed is Ni^+. The onset of photodissociation of internally cold ions provides an upper limit to the Ni^+-H_2O bond strength. The peak at 16840 cm^{-1} is due to transitions from $K_a'' = 1$ to $K_a' = 0$; therefore, the peak at 16875 cm^{-1}, corresponding to a transition from $K_a'' = 0$ to $K_a' = 1$, provides an upper limit to the Ni^+-H_2O bond strength of 2.092 eV. This upper limit is consistent with the guided ion beam study,[4] which gives $D_0(Ni^+-H_2O)$ = 1.87 ± 0.03 eV. The first observed peak lies well above the dissociation limit, suggesting that it is due to a transition to the ground vibrational state of the excited electronic state. In addition to the major progression, there is a series of less intense, single peaks spaced by ∼340 cm^{-1}. These may be due to a vibrational progression in a second electronic state, this time due to a parallel transition.

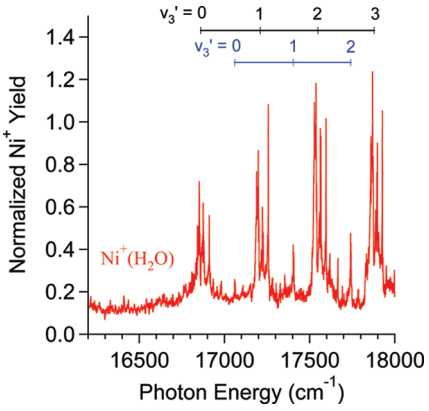

Figure 1. Photodissociation spectrum of $Ni^+(H_2O)$ with the Ni^+-H_2O stretch vibrational quantum numbers indicated.

Electronic structure calculations were carried out to determine the excited states involved in the observed transitions and the geometries and vibrational frequencies of the ground and excited electronic states. The calculations used Gaussian09.[17] The ground state was characterized at the CCSD(T)/aug-cc-pVTZ level of theory. $Ni^+(H_2O)$ is predicted to have C_{2v} symmetry and a $^2A_1$ ground state. The Ni−O bond length is r_{NiO} = 1.948 Å, the O−H bond lengths are 0.964 Å, and the H−O−H angle is 107.5°. Pioneering calculations by Rosi and Bauschlicher[18] using the modified coupled pair functional method predict the same ground state and similar geometry as do several more recent calculations.[19] Walters et al.[6c] performed DFT calculations at the B3LYP/6-311+G** level and determined that the ground state of $Ni^+(H_2O)$ is a $^2B_2$ state with r_{NiO} = 2.002 Å. We recalculated $Ni^+(H_2O)$ using the B3LYP/6-311+G** functional and obtain a $^2A_1$ ground state with r_{NiO} = 1.952 Å. Constraining the calculation to $^2B_2$ states gives a state 0.27 eV higher in energy with r_{NiO} = 2.002 Å. Rosi and Bauschlicher also note that the out-of-plane bending potential is very flat, which we observe as well. In fact, with some hybrid density functionals (e.g., B3LYP/6-311++G-(3df,p)), $Ni^+(H_2O)$ is even predicted to be slightly nonplanar. The molecule is a near-prolate top, and the CCSD(T) calculations predict rotational constants of A = 13.82 cm^{-1}, B = 0.300 cm^{-1}, and C = 0.294 cm^{-1}. The A constant is much larger than B or C as it is due to rotations about the Ni−O axis (the a axis). This has a very small moment of inertia as the hydrogen atoms are the only atoms not on this axis. In addition, time-dependent density functional theory (TD-DFT) was used to characterize excited electronic states of $Ni^+(H_2O)$. These calculations use the BHandHLYP functional with the 6-311++G(3df,p) basis set. This functional was used because it reproduces the energies of excited states of bare Ni^+ very well; the B3LYP functional underestimates excitation energies, particularly to $3d^84s$ states, suggesting that B3LYP overestimates the stability of the 4s orbital relative to the 3d. We observed the same effect with excited electronic states of V^+.[20] The ground-state geometry at the BHandHLYP/6-311++G-(3df,p) level is very similar to that calculated using the CCSD(T) method. Harmonic vibrational frequencies were calculated for the ground and excited electronic states at the BHandHLYP/6-311++G(3df,p) level and are shown in Table 1. Frequencies are scaled by 0.92 to match the experimental O−H stretches in bare H_2O. As will be discussed in detail later, the calculations predict two excited states near 17000 cm^{-1}, the 2^2A_2 and 3^2A_1 states. They have very similar geometries and

dx.doi.org/10.1021/jp211220v | J. Phys. Chem. A XXXX, XXX, XXX−XXX

Table 1. Calculated and Experimental Frequencies of $Ni^+(H_2O)$ in the Ground Electronic State[a]

vibrational symmetry	mode number	description	frequency (cm^{-1}) $Ni^+(H_2O)$ calculated	frequency (cm^{-1}) $Ni^+(H_2O)$ experimental	frequency (cm^{-1}) H_2O experimental
a_1	1	H−O−H symmetric stretch	3610	3616.5	3657
	2	H−O−H bend	1575	–	1595
	3	Ni−O stretch	388	–	
b_1	4	out-of-plane bend	200	–	
b_2	5	H−O−H antisymmetric stretch	3681	3688	3756
	6	in-plane bend	554	–	

[a]The frequencies are calculated using BHandHLYP/6-311G++(3df,p) and scaled by 0.92. The bare H_2O frequencies are also listed. Binding to Ni^+ causes the symmetric and antisymmetric O−H stretches in water to red shift by 40 and 68 cm^{-1}, respectively.

frequencies. The discussion focuses on the 2^2A_2 state as it is responsible for the most intense band.

The observed ~340 cm^{-1} vibrational progression can be readily assigned. $Ni^+(H_2O)$ has six vibrations. Three are slightly perturbed vibrations of H_2O, calculated to occur at 3681, 3610, and 1575 cm^{-1} for the ground state. For the excited state, the H_2O vibrations are predicted to be 3647, 3571, and 1568 cm^{-1}. The remaining vibrations correspond to metal−ligand stretches and bends and are at a much lower frequency. The in-plane and out-of-plane bends (essentially H_2O hindered rotations) are calculated at 554 and 200 cm^{-1} for the ground state, respectively. For the excited state, they are 521 and 272 cm^{-1}. Long progressions in these vibrations should only arise if the ground or excited state are significantly distorted from a planar C_{2v} geometry. They also involve motion perpendicular to the *a* axis and should lead to vibrations that alternate between perpendicular and parallel band rotational structure. Neither of these is the case. The observed progression is thus due to the metal−ligand stretch, a symmetric vibration with a calculated ground-state frequency of 388 cm^{-1} and an excited state frequency of 308 cm^{-1}. The electronic spectrum of $Co^+(H_2O)$ also shows extended progressions in the metal−ligand stretch, in several excited electronic states.[13]

To confirm the vibrational quantum numbering in the electronic spectra and whether the minor progression is due to a combination of the metal−ligand stretch and another vibration or to another electronic state, the photodissociation spectra of isotopomers of $Ni^+(H_2O)$ were measured. Unlike $Ni^+(H_2O)$, the photodissociation spectrum of $Ni^+(D_2O)$ does not show any resonant features. The photodissociation yield of $Ni^+(D_2O)$ is similar to that of $Ni^+(H_2O)$ when off-resonance (e.g., when the laser is tuned off of a peak). This suggests that the excited state of $Ni^+(D_2O)$ is too short-lived to show vibrational structure. Photodissociation of $Ni^+(HOD)$ also gave a broad spectrum. In a simple Fermi Golden Rule model, the rates of internal conversion and intersystem crossing depend on (a) the vibrational overlap between the initially excited state and vibrations of the accepting state and (b) the density of vibrational states of the accepting state.[21] Deuteration typically decreases the first factor and increases the second. By reducing the vibrational frequencies, deuteration raises the vibrational density of states. At ~17000 cm^{-1}, the density of vibrational states of $Ni^+(D_2O)$ is calculated to be a factor of 4 higher than that of $Ni^+(H_2O)$. For most organic molecules, the promoting vibrational modes show a large frequency shift upon deuteration. This leads to a substantial reduction in the vibrational overlap, which dominates the overall nonradiative rate, leading to significantly longer excited-state lifetimes for the deuterated compound (normal isotope effect). However, for Ni^+−water, the primary difference in geometry between the ground and excited states is in the metal−water stretch; therefore, this is the key vibration to consider. This vibration shows only a very small H/D isotope shift; therefore, the vibrational overlaps are likely to be similar for $Ni^+(H_2O)$ and $Ni^+(D_2O)$. Overall, it is thus likely that the higher density of states for $Ni^+(D_2O)$ dominates, leading to a higher nonradiative decay rate. Large inverse isotope effects have also been observed in some organic compounds such as anthracene, where the nonradiative decay rate at the S_1 origin increases by a factor of 15 upon complete deuteration.[22]

Instead, $^{60}Ni^+$ (26% natural abundance) was substituted for $^{58}Ni^+$ (68% natural abundance). This is expected to reduce the Ni−OH_2 stretching frequency by 0.28%, or 1.1 cm^{-1}. It is predicted to affect the other vibrations by <0.15 cm^{-1} as they primarily involve hydrogen motion. Figure 2 illustrates the isotopic shift observed when exchanging $^{58}Ni^+$ for $^{60}Ni^+$. It shows a 1.12 cm^{-1} shift per quantum and reaffirms that the first vibrational peak is indeed $\nu_3' = 0$. The same shifts are observed for the parallel band. Although this substitution is sufficient to determine quantum numbering, it could not to be used to determine if the parallel bands are due to a second electronic state or to a different vibrational progression. However, the calculations predict two nearly degenerate excited states in this region, one of which (the 3^2A_1 state) would give rise to a parallel band; therefore, the observed parallel bands are likely due to transitions to this electronic state.

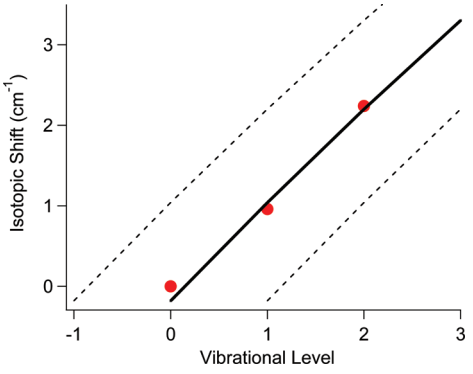

Figure 2. Assignment of Ni−H_2O stretch vibrational levels in the photodissociation spectrum of $Ni^+(H_2O)$. Experimental isotopic shifts of $^{58}Ni^+(H_2O)$ versus $^{60}Ni^+(H_2O)$ are compared to calculated shifts assuming that the vibrational numbering is as shown in Figure 1 (solid line) and with the numbering shifted by 1 (dashed lines).

Now that the quantum numbering is confirmed, the vibrational frequency and anharmonicity can be calculated. The results are summarized in Table 2. The excited state of $Ni^+(H_2O)$ accessed in this study correlates to electronically

dx.doi.org/10.1021/jp211220v | J. Phys. Chem. A XXXX, XXX, XXX−XXX

Table 2. Spectroscopic Constants and Dissociation Energies for $Ni^+(H_2O)$[a]

	$^2A_1$ ground state	2^2A_2 excited state	3^2A_1 excited state
T_{00} (cm^{-1})	0	16863	17060
ν_3 (cm^{-1})	388	354.5	349.4
x_3 (cm^{-1})	2.5	3.6	3.1
D_0 (eV)	1.87 ± 0.03	1.46	1.61

[a]The term value T_{00}, excited-state frequency (ν_3'), and anharmonicity (x_3') were determined from the photodissociation spectrum. The ground-state harmonic frequency (ν_3'') was calculated using BHandHLYP/6-311++G(3df,p), and the anharmonicity constant (x_3'') was calculated using eq 1. The ground-state D_0 was determined by Armentrout and co-workers,[4] while the excited state D_0 were determined using eq 2.

excited Ni^{+}* + H_2O. Which excited state is involved can be determined by estimating the adiabatic dissociation energy of the excited state. Treating the Ni^+-H_2O stretch as a Morse oscillator

$$D_e = \frac{\nu_3^2}{4x_3} \quad (1)$$

This calculation predicts D_e' = 1.08 eV. It would be more accurate to determine the excited-state bond length using a LeRoy–Bernstein plot, which takes into account the correct long-range Ni^+-H_2O interactions. This approach has been used for Co^+–rare gas complexes.[23] However, we cannot do that in this case as we do not measure excited vibrational states sufficiently close to the dissociation limit. Also, because the photodissociation spectrum consists of only four peaks, there is a large extrapolation resulting in large error bars in D_e'. The energy of the excited state of Ni^+ can be found by using eq 2 and solving for $\Delta E(Ni^{+}*)$.

$$D_0' = D_0'' + \Delta E(Ni^{+}*) - T_{00} \quad (2)$$

The D_0'' term was determined by Armentrout and co-workers to be 1.87 ± 0.03 eV,[4] and T_{00} was found experimentally to be 2.09 eV. While $\Delta E(Ni^{+}*)$ = 1.30 eV has large uncertainty, it is still sufficient to identify the excited state of Ni^+ as Ni^+ has few excited doublet states. The first excited electronic state is $3d^84s,^2F_{7/2}$ at 1.68 eV. Having identified this state, D_0' can be recalculated more accurately via eq 2. The upper $Ni^+(H_2O)$ state is bound by D_0' = 1.46 eV. This is smaller than the binding energy of the ground state, 1.87 ± 0.03 eV. The Ni^+-H_2O stretching potentials of the upper and lower states are summarized in Figure 3.

Intensities in the vibrational progression reflect the change in the $Ni-OH_2$ bond length on electronic excitation. These intensities can be calculated by solving the one-dimensional Schrödinger equation along the Ni–O stretch coordinate. The molecule is treated as a pseudodiatomic, with the H_2O as a single "atom" with mass 18 amu. To determine Δr_{Ni-O} from the experimental intensities, we model the ground electronic state as a Morse oscillator with the scaled BHandHLYP vibrational frequency and experimental dissociation energy. For the excited state, we use a Morse oscillator with the experimental frequency and dissociation energy and then vary Δr_{Ni-O} until the best match is found between the calculated and measured intensities. This corresponds to a change in the metal–ligand bond length Δr_{Ni-O} = 0.20 ± 0.02 Å. Although this analysis does not identify the sign of Δr_{Ni-O}, it is clear from the rotational structure that the bond length increases upon electronic excitation.

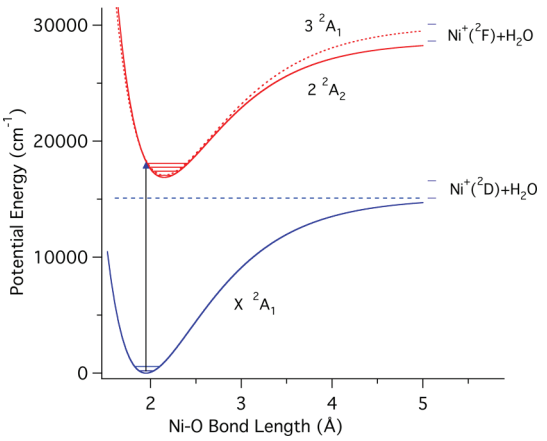

Figure 3. Potential energy curves of the ground and excited electronic state of $Ni^+(H_2O)$ along the $Ni-H_2O$ stretch based on experiment.

TD-DFT calculations were carried out to characterize the potential energy surfaces for the ground and excited electronic states of $Ni^+(H_2O)$ along the metal–ligand stretch coordinate (Figure 4). These calculations use the BHandHLYP functional

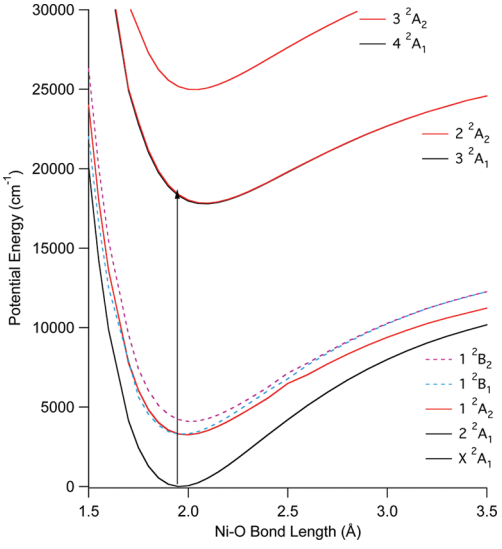

Figure 4. Calculated potential energy curves for doublet states of $Ni^+(H_2O)$ along the $Ni-H_2O$ stretch. Points are calculated using TD-DFT at the BHandHLYP/6-311++G(3df,p) level.

with the 6-311++G(3df,p) basis set. Low-lying molecular orbitals of $Ni^+(H_2O)$ are shown in Figure 5. As expected,[18] the highest occupied orbitals are essentially metal-centered 3d orbitals, and the lowest unoccupied orbital is primarily a metal 4s. In the $^2A_1$ ground state, the $3d\sigma(z^2)$ orbital is only singly occupied. Promoting an electron from another 3d orbital into the $3d\sigma(z^2)$ results in the four low-lying excited states near 4000 cm^{-1}. Two excited states are predicted in the energy range of our study, the 3^2A_1 and 2^2A_2 states. They correspond to transitions of β electrons from $9a_1$ ($3d\delta(x^2-y^2)$ on the metal) and $1a_2$ ($3d\delta(xy)$ on the metal) nonbonding orbitals to $11a_1$ ($4s\sigma$ orbital on the metal) (Figure 5). The $3d\delta(x^2-y^2)$ and $3d\delta(xy)$ orbitals would be degenerate if one ignores the hydrogens; they are very nearly degenerate as they have δ

dx.doi.org/10.1021/jp211220v | J. Phys. Chem. A XXXX, XXX, XXX–XXX

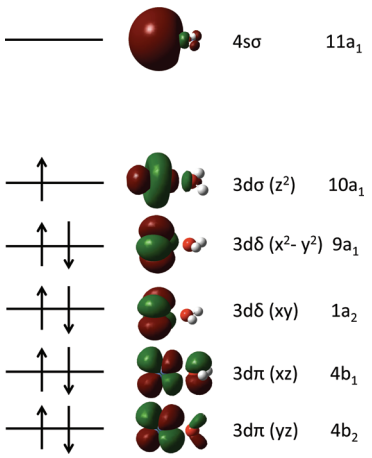

Figure 5. Molecular orbital diagram and electron occupancy of $Ni^+(H_2O)$ ($X,^2A_1$).

symmetry and do not participate in bonding. The calculations also predict that the transition from the ground state to the 3^2A_1 excited state has an integrated oscillator strength of f = 0.0001 and is a parallel transition. At the equilibrium C_{2v} geometry, the transition to the 2^2A_2 electronic state is predicted to have zero intensity as it is symmetry-forbidden. However, transitions to this excited state can be observed if vibronic coupling is included.[24] The oscillator strength is dominated by vibronic transitions involving the two b_2 vibrations, giving a total integrated oscillator strength of f = 0.0004. Transitions to the 2^2A_2 state would be perpendicular. Including vibronic coupling has little effect on the intensity of the transition to the 3^2A_1 state. We assign the more intense perpendicular progression band to transitions to the 2^2A_2 state and the weaker parallel bands to the 3^2A_1 state.

By numerically solving the Schrödinger equation on the calculated TD-DFT potential for the 2^2A_2 excited state, we obtain ν_3' = 337 cm^{-1} and x_3' = 3.9 cm^{-1}, in good accord with experiment. The TD-DFT calculation slightly underestimates the change in the Ni−O bond length, predicting Δr_{Ni-O} = 0.15 Å, compared to the experimental value of Δr_{Ni-O} = 0.20 ± 0.02 Å. The excited states observed correlate to Ni^+ states with an electron configuration of $3d^84s^1$. These excited states of $Ni^+(H_2O)$ have a longer Ni−O bond than the ground state as they are formed by promotion of an electron from a nonbonding 3d orbital perpendicular to the Ni−O bond to the nearly spherical and, hence, more repulsive 4s orbital.

B. Electronic Spectroscopy: Rotational Structure. The rotational structure in the electronic spectrum reflects rotational constants (and hence the geometry) and spin−rotational interaction of the ground and excited electronic states of $Ni^+(H_2O)$. The $Ni^+(H_2O)$ ion is a near-symmetric prolate top, and the major progression observed in the electronic spectrum is a perpendicular transition, with the transition moment perpendicular to the a axis (the Ni−O bond). The Hamiltonian for rotation for this open-shell system can be written as[25]

$$\boldsymbol{H} = \boldsymbol{H}_{rot} + \boldsymbol{H}_{spin-rot} \quad (3)$$

where

$$\boldsymbol{H}_{rot} = A\boldsymbol{N}_a^2 + B\boldsymbol{N}_b^2 + C\boldsymbol{N}_c^2 \quad (4)$$

$$\boldsymbol{H}_{spin-rot} = \frac{1}{2}\sum_{\alpha,\beta}\varepsilon_{\alpha,\beta}(\boldsymbol{N}_\alpha S_\beta + S_\beta \boldsymbol{N}_\alpha) \quad (5)$$

where $\boldsymbol{N}$ is the rotational angular momentum and S is the spin angular momentum, A, B, and C are the rotational constants, and $\varepsilon_{\alpha,\beta}$ are the components of the spin−rotation tensor in the inertial axis system (a,b,c). The indices α and β range over a,b,c. For a symmetric prolate top, the eigenvalues of $\boldsymbol{H}_{rot}$ are given by the usual expression

$$E_{J,K_a} = \left(A - \frac{B+C}{2}\right)K_a^2 + \left(\frac{B+C}{2}\right)J(J+1) \quad (6)$$

where K_a is the quantum number for rotation about the a axis and J denotes rotation about the b/c axis. The selection rules for a perpendicular band are $\Delta K_a = \pm 1$ and $\Delta J = 0, \pm 1$. Figure 6 focuses on the $\nu_3' = 1 \leftarrow \nu_3'' = 0$ region of the electronic spectrum and reveals the partially resolved rotational structure. The three major peaks are labeled by the K_a quantum numbers. The structure within each peak is due to J and to the spin−rotation interaction, ε

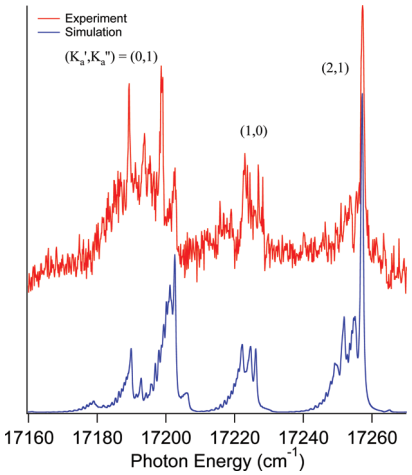

Figure 6. A fine scan of the $2^2A_2(\nu_3'=1) \leftarrow X^2A_1$ band of $Ni^+(H_2O)$ showing the $\Delta K_a = \pm 1$ features characteristic of a perpendicular transition. A simulated spectrum is also shown, using the spectroscopic parameters in Table 3, a rotational temperature of 15 K, and a Lorentzian line width of 0.6 cm^{-1}.

The spin−rotation interaction parameter ε is due to two effects, (1) coupling of the electron spin to the magnetic field due to the rotation of the molecule and (2) second-order interaction between the spin−orbit coupling and the Coriolis interaction.[25b] The second term dominates. Although ε is rigorously a tensor and should have components along each rotational axis and each pair of axes, ε_{aa} is much larger than the other components as the A constant is much larger than B or C; therefore, we neglect the other components and only fit ε_{aa}. The spin−orbit splitting is 603 cm^{-1} for the ^2D ground state and 413 cm^{-1} for the ^2F excited states of Ni^+. This large spin−orbit coupling leads to fairly large ε_{aa} constants. Including ε_{aa} modifies the energies given by eq 6. A perturbation treatment shows that it introduces an additional term proportional to $\varepsilon_{aa}K_a\Sigma$, which leads to broadening in peaks with $K_a > 0$ as the projection of the spin angular momentum onto the a axis is $\Sigma = \pm 1/2$. It also leads to a term proportional to K_a^2, which affects the apparent A rotational constant.[10,26]

dx.doi.org/10.1021/jp211220v | J. Phys. Chem. A XXXX, XXX, XXX−XXX

For a molecule with C_{2v} geometry and two equivalent protons, nuclear spin statistics result in a 3:1 degeneracy for states with overall odd/even spatial symmetry. The overall spatial symmetry is a product of the electronic, vibrational, and rotational wave functions.[27] The calculations predict that the ground state is $^2A_1$. For states with A symmetry, the electronic wave function is totally symmetrical upon rotation about the a axis. The vibrational wave function is symmetrical for the ground vibrational state and for all a_1 vibrations. The two hydrogen atoms in $Ni^+(H_2O)$ are interchanged by applying a C_2 rotation about the a axis; therefore, the rotational wave function has even symmetry for states with K_a even and odd symmetry for states with K_a odd. At the temperature of the molecular beam, molecules are cooled to $K_a'' = 0$ and 1. Further cooling from $K_a'' = 1$ to 0 is very inefficient as it involves changing nuclear spin. Thus, weights of 3:1 (K_a'' odd/even) were incorporated in the simulations. The simulation correctly predicts the relative intensities observed for transitions from $K_a'' = 0$ and 1, confirming that the ground electronic state has A symmetry.

The rotational structure was fit using the *spfit* and *spcat* programs.[28] The results are shown in Figure 6, and the parameters are in Table 3. Anharmonic frequency calculations

Table 3. Rotational Constants for the Ground and Excited Electronic States of $Ni^+(H_2O)$[a]

	$^2A_1$ ground state	2^2A_2 excited state
A (cm^{-1})	13.8[b]	14.5 ± 0.2
B (cm^{-1})	0.300[b]	0.255 ± 0.015
C (cm^{-1})	0.294[b]	0.249[c]
ε (cm^{-1})	−12 ± 5	−3 ± 1

[a]The experimental rotational constants were determined by simulating the rotational structure in the vibrational and electronic spectrum. [b]Calculated CCSD(T)/aug-cc-pVTZ values. [c]B−C fixed at the ground-state value.

show that the metal−ligand stretch vibration has negligible effect on the A constant, as expected, and only a small effect on B and C. As a result, spectra for transitions to $\nu_3' = 0$−3 show very similar rotational structure. The resolution of the photodissociation spectrum is limited to 0.6 cm^{-1} due to the excited state lifetime. As a result, individual J transitions are not resolved, and the B and C rotational constants cannot be accurately determined. The simulations are only sensitive to the change in B and C upon electronic excitation. Also, fits of the rotational constant A and spin−rotation constant ε_{aa} are correlated as their effect on the energies is proportional to K_a^2. Therefore, in the fits, the ground-state rotational constants were set to the CCSD(T)/aug-cc-pVTZ calculated values. The difference $B' - C'$ is very small and was set at the calculated ground-state value. The ground- and excited-state spin−rotation constants as well as the excited-state rotational constants A' and B' were determined by fitting the spectrum.

Spin−rotation interaction broadens peaks with $K_a > 0$; therefore, we determined $\varepsilon_{aa}'' = -12$ cm^{-1} by fitting the structure in the $K_a' = 0 \leftarrow K_a'' = 1$ peak, in particular, the spacing between the features at 17189 cm^{-1} and 17202 cm^{-1}. The upper state constant $\varepsilon_{aa}' = -3$ cm^{-1} reproduces the width in the $K_a' = 1 \leftarrow K_a'' = 0$ peak. In the absence of spin−rotation interaction, the spacing between the $K_a' = 0 \leftarrow K_a'' = 1$ and the $K_a' = 2 \leftarrow K_a'' = 1$ transitions is $4A'$. In the present case, ε_{aa}' affects this spacing. Once ε_{aa}' has been determined, A' is obtained by fitting this spacing. This gives $A' = 14.5 \pm 0.2$ cm^{-1}, where the uncertainty includes the cross-correlation. The shape of the sharp $K_a' = 2 \leftarrow K_a'' = 1$ peak is very sensitive to $\Delta B = B' - B''$. We obtain $\Delta B = -0.045 \pm 0.015$ cm^{-1}. The rotational constants B and C primarily depend on the Ni−O bond length; therefore, this corresponds to an increase of $\Delta r_{NiO} = 0.17 \pm 0.07$ Å. This agrees with $\Delta r_{NiO} = 0.20 \pm 0.02$ Å from the vibrational analysis. The A rotational constant depends on the O−H bond length and H−O−H angle. The CCSD(T) calculations predict that when H_2O binds to Ni^+, r_{OH} increases by only 0.003 Å, while ∠HOH increases by 3.3°. Electronic excitation of the $Ni^+(H_2O)$ should have even less effect on r_{OH}. Assuming that r_{OH} remains at the calculated ground-state value, $A' = 14.5 \pm 0.2$ cm^{-1} corresponds to ∠HOH = 104 ± 1°. This is 3° smaller than the calculated value for the ground state. In bare H_2O, ∠HOH = 104.5°, which is significantly smaller than the tetrahedral value of 109.5° due to repulsion between the O−H bonding electrons and the unpaired electrons on oxygen. When a cation binds to water, it removes electron density from the oxygen, resulting in an increase in ∠HOH. This effect is stronger at smaller metal−oxygen bond lengths. Hence, the more tightly bound $^2A_1$ ground state of $Ni^+(H_2O)$ has a larger ∠HOH than the ground state. The value of ∠HOH in $Ni^+(H_2O)$ is similar to that in $Ca^+(H_2O)$,[9] 106.8°, while the smaller Mg^+ ion leads to ∠HOH = 110.6° in $Mg^+(H_2O)$.[7b]

One surprising result of this study is that $\varepsilon_{aa}' = -3$ cm^{-1} is so small. There are three molecules $M^+(H_2O)$ for which the rotational structure in the electronic spectrum has previously been analyzed, $Mg^+(H_2O)$,[7b] $Ca^+(H_2O)$,[9,10] and $Zn^+(H_2O)$.[14] They have a $^2A_1$ ground state, where the unpaired electron is on the metal. In these molecules, the electronic transitions observed are to the p_x and p_y orbitals on the metal, forming the $^2B_1$ and $^2B_2$ excited states. In the $^2A_1$ ground state, ε_{aa}'' is assumed and observed to be 0 as the unpaired electron has no orbital angular momentum. For the excited states, ε_{aa}' can be accurately estimated using a pure precession model[26] in which rotation about the a axis mixes the p_x and p_y orbitals and hence the $^2B_1$ and $^2B_2$ states. Using perturbation theory, this model predicts[10]

$$\varepsilon_{aa} \approx \frac{4AA^{SO}\Lambda^2}{\Delta E} \tag{7}$$

where A is the rotational constant, A^{SO} is the spin−orbit splitting of the atom in the molecule (typically ∼85% of the value in the isolated atom), $\Lambda = 1$ for a p_x or p_y orbital, and ΔE is the spacing between the $^2B_1$ and $^2B_2$ states, which is determined from the spectrum. In $Ni^+(H_2O)$, the 2^2A_2 and 3^2A_2 states differ in having an unpaired electron in the $1a_2$ ($3d\delta(xy)$) and $9a_1$ ($3d\delta(x^2-y^2)$) orbital, respectively. A 90° rotation about the a axis interconverts these orbitals. If we apply the precession model to the 3^2A_2 state of $Ni^+(H_2O)$, A^{SO} is approximately 85% of the value for $Ni^+{}^2F,3d^84s$, or 350 cm^{-1}, $\Lambda = 2$ for a $d\delta$ orbital, and $\Delta E = -197$ cm^{-1}, which gives $\varepsilon_{aa}' \approx -400$ cm^{-1}, about 2 orders of magnitude larger than is observed. This value is so large due to the small energy splitting between the states and the large spin−orbit interaction. It is not clear why the pure precession model fails to predict ε_{aa}' in this system, but it is likely because several excited states of $Ni^+(H_2O)$ contribute to ε_{aa}' and some of these contributions cancel.

C. Vibrational Spectroscopy. Vibrationally mediated photodissociation (VMP) was used to probe the O−H

dx.doi.org/10.1021/jp211220v | J. Phys. Chem. A XXXX, XXX, XXX−XXX

stretching vibrations in the ground electronic state of $Ni^+(H_2O)$ in a depletion experiment. The visible laser is set to a desired transition, and the IR laser, which fires 40 ns before the visible laser, is scanned. When the IR laser is resonant with a vibrational transition such as the O−H antisymmetric stretch, some molecules are vibrationally excited, which removes population from the ground state. This will lead to less photodissociation if vibrationally excited molecules have a different resonant frequency than the unexcited molecules and hence are less likely to absorb the visible light. Figure 7 shows

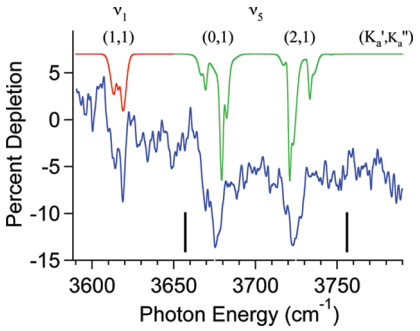

Figure 7. Vibrational action spectrum of $Ni^+(H_2O)$ in the O−H stretching region. The spectrum is obtained by monitoring depletion in the Ni^+ photofragment produced by irradiation of the $2^2A_2(\nu'=1,K_a'=2) \leftarrow X^2A_1(\nu''=0,K_a''=1)$ transition at 17257 cm^{-1}. IR absorption removes molecules from $\nu'' = 0$, leading to a 10−15% reduction in the fragment yield. Transitions are observed to the symmetric O−H stretch ν_1 near 3620 cm^{-1} (parallel band, with $\Delta K_a = 0$) and to the antisymmetric O−H stretch ν_5 near 3675 and 3725 cm^{-1} (perpendicular band, with $\Delta K_a = \pm 1$). A simulated spectrum is also shown, using the spectroscopic parameters in Table 3. Vertical bars denote the positions of the symmetric and antisymmetric stretches in bare H_2O.

the results of a depletion experiment with the visible laser tuned to the (2,1) $\nu_3' = 1$ transition at 17257 cm^{-1}. This double resonance experiment only monitors transitions from $K_a'' = 1$. In the vibrational spectrum, the O−H symmetric stretch ν_1 is a parallel transition, with the selection rules $\Delta K_a = 0$ and $\Delta J = \pm 1$. This is observed as a doublet at 3619 cm^{-1}. The O−H antisymmetric stretch ν_5 is a perpendicular transition. Two absorptions are observed, (0,1) at 3675 cm^{-1} and (2,1) at 3723 cm^{-1}. The maximum depletion observed is only ∼15%. As a result, this spectrum is substantially noisier than the electronic photodissociation spectrum. In principle, better signal-to-noise could be obtained from an enhancement experiment in which the visible laser is set to be resonant with an absorption of the vibrationally excited molecules. We have previously used this approach to measure vibrational spectra of $V^+(OCO)$.[29] The IR laser is first set to an absorption, and the visible laser is scanned. The difference between the resulting spectrum and one with the IR laser off (or tuned off-resonance) gives the photodissociation spectrum of vibrationally excited molecules. For small molecules such as $V^+(OCO)$, this often has well-defined peaks.[20] In the present study, the IR laser was set to 3723 cm^{-1} and the visible laser scanned in the region of the $\nu_3' = 1$ band. Unfortunately, we find that the resulting vibrationally mediated photodissociation[30] spectrum consists mainly of broad, nonresonant photodissociation, although slightly enhanced dissociation in the presence of the IR is seen at 17175 cm^{-1}. Setting the visible to this energy and scanning the IR laser gives 30% enhancement at 3725 cm^{-1}. In larger molecules, the vibrationally excited molecules typically exhibit a broad photodissociation spectrum due to efficient intramolecular vibrational relaxation (IVR).[31] This process should be slow in a molecule as small as $Ni^+(H_2O)$ due to the low vibrational density of states near 3700 cm^{-1}. One possible mechanism for state mixing is coupling to one of the four excited electronic states calculated to lie in this energy range (Figure 4).

The rotational structure in the vibrational spectra was also fit using the *spfit* and *spcat* programs.[28] These fits assume that the visible laser overlaps all of the thermally populated J states so that the double resonance experiment selects states with specific K_a'' and does not select J''. For the vibrational simulations, we again use the calculated rotational constants for the ground state. Vibrational excitation is expected to slightly affect the rotational constants. This effect was estimated by carrying out anharmonic vibrational frequency calculations at the BHandHLYP/6-311++G(3df,p) level and obtaining the change in the rotational constants upon vibrational excitation. This is sufficiently accurate given the modest resolution of the vibrational spectra. The calculations predict $\Delta A = -0.44$ cm^{-1} and $\Delta B,C = -0.002$ cm^{-1} for the symmetric O−H stretch and $\Delta A = -0.34$ cm^{-1} and $\Delta B,C = -0.002$ cm^{-1} for the antisymmetric O−H stretch. The parameters that were varied are ε_{aa}, which was assumed to be the same for the ground and excited vibrational states, the temperature, and the vibrational frequency. Simulations of the symmetric stretch band are insensitive to ε_{aa}; therefore, they are used to determine a rotational temperature $T = 15 \pm 5$ K and $\nu_1 = 3616.5 \pm 0.5$ cm^{-1}. This is a red shift of 40 cm^{-1} from bare water. The antisymmetric stretch band is slightly sensitive to ε_{aa}. The simulation shown in Figure 7 uses $\varepsilon_{aa} = -12$ cm^{-1}, which is the optimum value found for the ground electronic state in the electronic spectrum. Slightly better agreement with the vibrational spectrum is obtained with $\varepsilon_{aa} = -7$ cm^{-1}, hence the relatively large uncertainty in ε_{aa} in Table 3. With both values, we obtain $\nu_5 = 3688$ cm^{-1}, which is red shifted by 68 cm^{-1} from the value for bare water.

The BHandHLYP calculations predict that binding of H_2O to Ni^+ produces a red shift of 53 cm^{-1} for the symmetric and 74 cm^{-1} for the antisymmetric O−H stretch, in good agreement with the experiment. The red shifts can be explained in terms of inductive effects. Upon complexation, the Ni^+ atom removes electron density from the oxygen lone pair in H_2O, weakening the O−H bonds and increasing the H−O−H bond angle. This effect has been observed for many $M^+(H_2O)$ complexes.[6,13]

Walters, Pillai, and Duncan studied the vibrational spectroscopy of $Ni^+(H_2O)(Ar)_2$ and complemented those studies with DFT calculations.[6c] Experimentally, they determined the O−H symmetric stretch to be 3623 cm^{-1}, which is in excellent agreement with the value of 3616.5 cm^{-1} obtained in this study. Their antisymmetric stretch frequency is also in excellent agreement. Duncan and co-workers determined it to be 3696 cm^{-1}, and the value found in this study is 3688 cm^{-1}. The addition of argon slightly reduces the extent of an electron withdrawing from oxygen by Ni^+, leading to a smaller red shift in the O−H stretches.

4. SUMMARY AND CONCLUSIONS

The electronic spectrum of $Ni^+(H_2O)$ and its vibrational spectrum in the O−H stretching region were measured using photodissociation. The O−H stretches are observed at $\nu_1 = 3616.5$ cm^{-1} for the symmetric stretch and $\nu_5 = 3688$ cm^{-1} for the antisymmetric stretch. This corresponds to a 40 cm^{-1} red

dx.doi.org/10.1021/jp211220v | J. Phys. Chem. A XXXX, XXX, XXX−XXX

shift for the symmetric stretch and 68 cm^{-1} red shift for the antisymmetric stretch, relative to bare H_2O. Rotational analysis also shows that binding to the metal increases the H−O−H angle due to removal of electron density from the oxygen lone pair. The electronic spectrum of $Ni^+(H_2O)$ in the 550−630 nm region shows transitions to two electronic states, 2^2A_2 and 3^2A_1. The photodissociation onset gives an upper limit to the Ni^+−H_2O bond strength of 2.09 eV, consistent with the guided ion beam value of $D_0(Ni^+-H_2O) = 1.87 \pm 0.03$ eV.[4] The electronic spectra show long progressions in the excited-state metal−ligand stretch, with $\nu_3' = 354.5$ cm^{-1} and $x_3' = 3.6$ cm^{-1} for the 2^2A_2 state.

The ground state of $Ni^+(H_2O)$ is formed by attachment of water to ground-state $Ni^+(3d^9,{}^2D)$. The excited electronic states observed here correlate to $Ni^{+*}(3d^84s,{}^2F) + H_2O$. Electronic excitation involves promoting a 3d electron to the 4s orbital. The 4s orbital is larger, and the promotion increases the repulsion between the metal and the oxygen lone pair. As a result, the $3d^84s$ states of Ni^+ bind H_2O less strongly than the ground $3d^9$ state. This is reflected in the reduced bond strength (1.46 versus 1.87 eV), an increase in the Ni−O bond length of 0.20 Å, and relaxation of the H−O−H bond angle to 104°, close to its value in bare H_2O. We have also studied $Co^+(H_2O)$, measuring the electronic spectrum, the O−H stretching frequencies, geometric changes upon excitation, and binding energies in order to examine periodic trends.[13]

AUTHOR INFORMATION

Present Address

[†]Department of Chemistry, University of California San Diego, 9500 Gilman Dr., La Jolla, CA 92093.

ACKNOWLEDGMENTS

Financial support from the National Science Foundation under Award CHE-0911225 is gratefully acknowledged.

REFERENCES

(1) Jabri, E.; Carr, M. B.; Hausinger, R. P.; Karplus, P. A. *Science* **1995**, *268*, 998.

(2) Dixon, N. E.; Riddles, P. W.; Gazzola, C.; Blakeley, R. L.; Zerner, B. *Can. J. Biochem.* **1980**, *58*, 1335.

(3) Beyer, M. K. *Mass Spectrom. Rev.* **2007**, *26*, 517.

(4) (a) Dalleska, N. F.; Honma, K.; Sunderlin, L. S.; Armentrout, P. B. *J. Am. Chem. Soc.* **1994**, *116*, 3519. (b) Armentrout, P. B.; Kickel, B. L., Gas-Phase Thermochemistry of Transition Metal Ligand Systems: Reassessment of Values and Periodic Trends. In *Organometallic Ion Chemistry*; Freiser, B. S., Ed.; Kluwer Academic Publishers: Dordrecht, The Netherlands, 1994; pp 1−45.

(5) (a) Lessen, D.; Brucat, P. J. *Chem. Phys. Lett.* **1988**, *152*, 473. (b) Asher, R. L.; Bellert, D.; Buthelezi, T.; Brucat, P. J. *Chem. Phys. Lett.* **1994**, *228*, 599. (c) Bellert, D.; Buthelezi, T.; Lewis, V.; Dezfulian, K.; Brucat, P. J. *Chem. Phys. Lett.* **1995**, *240*, 495. (d) Asher, R. L.; Bellert, D.; Buthelezi, T.; Weerasekera, G.; Brucat, P. J. *Chem. Phys. Lett.* **1994**, *228*, 390.

(6) (a) Walters, R. S.; Duncan, M. A. *Aust. J. Chem.* **2004**, *57*, 1145. (b) Walker, N. R.; Walters, R. S.; Tsai, M. K.; Jordan, K. D.; Duncan, M. A. *J. Phys. Chem. A* **2005**, *109*, 7057. (c) Walters, R. S.; Pillai, E. D.; Duncan, M. A. *J. Am. Chem. Soc.* **2005**, *127*, 16599. (d) Vaden, T. D.; Lisy, J. M.; Carnegie, P. D.; Pillai, E. D.; Duncan, M. A. *Phys. Chem. Chem. Phys.* **2006**, *8*, 3078. (e) Carnegie, P. D.; Bandyopadhyay, B.; Duncan, M. A. *J. Phys. Chem. A* **2008**, *112*, 6237. (f) Carnegie, P. D.; McCoy, A. B.; Duncan, M. A. *J. Phys. Chem. A* **2009**, *113*, 4849. (g) Carnegie, P. D.; Bandyopadhyay, B.; Duncan, M. A. *J. Chem. Phys.* **2011**, *134*, 014302. (h) Carnegie, P. D.; Bandyopadhyay, B.; Duncan, M. A. *J. Phys. Chem. A* **2011**, *115*, 7602.

(7) (a) Yeh, C. S.; Willey, K. F.; Robbins, D. L.; Pilgrim, J. S.; Duncan, M. A. *Chem. Phys. Lett.* **1992**, *196*, 233. (b) Willey, K. F.; Yeh, C. S.; Robbins, D. L.; Pilgrim, J. S.; Duncan, M. A. *J. Chem. Phys.* **1992**, *97*, 8886.

(8) Misaizu, F.; Sanekata, M.; Tsukamoto, K.; Fuke, K.; Iwata, S. *J. Phys. Chem.* **1992**, *96*, 8259.

(9) Scurlock, C. T.; Pullins, S. H.; Reddic, J. E.; Duncan, M. A. *J. Chem. Phys.* **1996**, *104*, 4591.

(10) Ishikawa, H.; Nakano, T.; Eguchi, T.; Shibukawa, T.; Fuke, K. *Chem. Phys. Lett.* **2011**, *514*, 234.

(11) (a) Donnelly, S. G.; Schmuttenmaer, C. A.; Qian, J.; Farrar, J. M. *J. Chem. Soc., Faraday Trans.* **1993**, *89*, 1457. (b) Sperry, D. C.; Midey, A. J.; Lee, J. I.; Qian, J.; Farrar, J. M. *J. Chem. Phys.* **1999**, *111*, 8469. (c) Farrar, J. M. *Int. Rev. Phys. Chem.* **2003**, *22*, 593.

(12) Lessen, D. E.; Asher, R. L.; Brucat, P. J. *J. Chem. Phys.* **1990**, *93*, 6102.

(13) Kocak, A.; Austein-Miller, G.; Pearson III, W. L.; Altinay, G.; Metz, R. B. 2012, to be submitted.

(14) Abate, Y.; Kleiber, P. D. *J. Chem. Phys.* **2005**, *122*, 084305.

(15) (a) Husband, J.; Aguirre, F.; Ferguson, P.; Metz, R. B. *J. Chem. Phys.* **1999**, *111*, 1433. (b) Metz, R. B. *Adv. Chem. Phys.* **2008**, *138*, 331.

(16) Kaur, D.; Desouza, A. M.; Wanna, J.; Hammad, S. A.; Mercorelli, L.; Perry, D. S. *Appl. Opt.* **1990**, *29*, 119.

(17) Frisch, M. J.; Trucks, G. W.; Schlegel, H. B.; Scuseria, G. E.; Robb, M. A.; Cheeseman, J. R.; Scalmani, G.; Barone, V.; Mennucci, B.; Petersson, G. A.; Nakatsuji, H.; Caricato, M.; Li, X.; Hratchian, H. P.; Izmaylov, A. F.; Bloino, J.; Zheng, G.; Sonnenberg, J. L.; Hada, M.; Ehara, M.; Toyota, K.; Fukuda, R.; Hasegawa, J.; Ishida, M.; Nakajima, T.; Honda, Y.; Kitao, O.; Nakai, H.; Vreven, T.; Montgomery Jr., J. A.; Peralta, J. E.; Ogliaro, F.; Bearpark, M.; Heyd, J. J.; Brothers, E.; Kudin, K. N.; Staroverov, V. N.; Keith, T.; Kobayashi, R.; Normand, J.; Raghavachari, K.; Rendell, A.; Burant, J. C.; Iyengar, S. S.; Tomasi, J.; Cossi, M.; Rega, N.; Millam, J. M.; Klene, M.; Knox, J. E.; Cross, J. B.; Bakken, V.; Adamo, C.; Jaramillo, J.; Gomperts, R.; Stratmann, R. E.; Yazyev, O.; Austin, A. J.; Cammi, R.; Pomelli, C.; Ochterski, J. W.; Martin, R. L.; Morokuma, K.; Zakrzewski, V. G.; Voth, G. A.; Salvador, P.; Dannenberg, J. J.; Dapprich, S.; Daniels, A. D.; Farkas, O.; Foresman, J. B.; Ortiz, J. V.; Cioslowski, J.; Fox, D. J. *Gaussian 09*; Gaussian, Inc.: Wallingford, CT, 2010.

(18) Rosi, M.; Bauschlicher, C. W. Jr. *J. Chem. Phys.* **1989**, *90*, 7264.

(19) Klippenstein, S. J.; Yang, C.-N. *Int. J. Mass Spectrom.* **2000**, *201*, 253.

(20) Citir, M.; Metz, R. B. *J. Chem. Phys.* **2008**, *128*, 024307.

(21) Avouris, P.; Gelbart, W. M.; El-Sayed, M. A. *Chem. Rev.* **1977**, *77*, 793.

(22) (a) Amirav, A.; Horwitz, C.; Jortner, J. *J. Chem. Phys.* **1988**, *88*, 3092. (b) Baba, M.; Saitoh, M.; Taguma, K.; Shinohara, K.; Yoshida, K.; Semba, Y.; Kasahara, S.; Nakayama, N.; Goto, H.; Ishimoto, T.; Nagashima, U. *J. Chem. Phys.* **2009**, *130*, 134315.

(23) (a) Lessen, D.; Brucat, P. J. *J. Chem. Phys.* **1989**, *90*, 6296. (b) Buthelezi, T.; Bellert, D.; Lewis, V.; Brucat, P. J. *Chem. Phys. Lett.* **1995**, *242*, 627. (c) Mosley, J. D.; Cheng, T. C.; Hasbrouck, S. D.; Ricks, A. M.; Duncan, M. A. *J. Chem. Phys.* **2011**, *135*, 104309.

(24) Rocha, A. B.; Bielschowsky, C. E. *Chem. Phys.* **2000**, *253*, 51.

(25) (a) Brown, J. M.; Sears, T. J. *J. Mol. Spectrosc.* **1979**, *75*, 111. (b) Tarczay, G.; Gopalakrishnan, S.; Miller, T. A. *J. Mol. Spectrosc.* **2003**, *220*, 276.

(26) Whitham, C. J.; Jungen, C. *J. Chem. Phys.* **1990**, *93*, 1001.

(27) Ellis, A. M.; Feher, M.; Wright, T. G., *Electronic and Photoelectron Spectroscopy: Fundamentals and Case Studies*; Cambridge University Press: Cambridge, U.K., 2005; p 285.

(28) Pickett, H. M. *J. Mol. Spectrosc.* **1991**, *148*, 371.

(29) Citir, M.; Altinay, G.; Metz, R. B. *J. Phys. Chem. A* **2006**, *110*, 5051.

(30) (a) Crim, F. F. *Annu. Rev. Phys. Chem.* **1993**, *44*, 397. (b) Rosenwaks, S., *Vibrationally Mediated Photodissociation*; Royal Society of Chemistry: Cambridge, U.K., 2009; p 204.

(31) Rizzo, T. R.; Stearns, J. A.; Boyarkin, O. V. *Int. Rev. Phys. Chem.* **2009**, *28*, 481.